ボース・アインシュタイン凝縮の最近の進展と今後の展望

東工大　　斎藤弘樹, 上田正仁
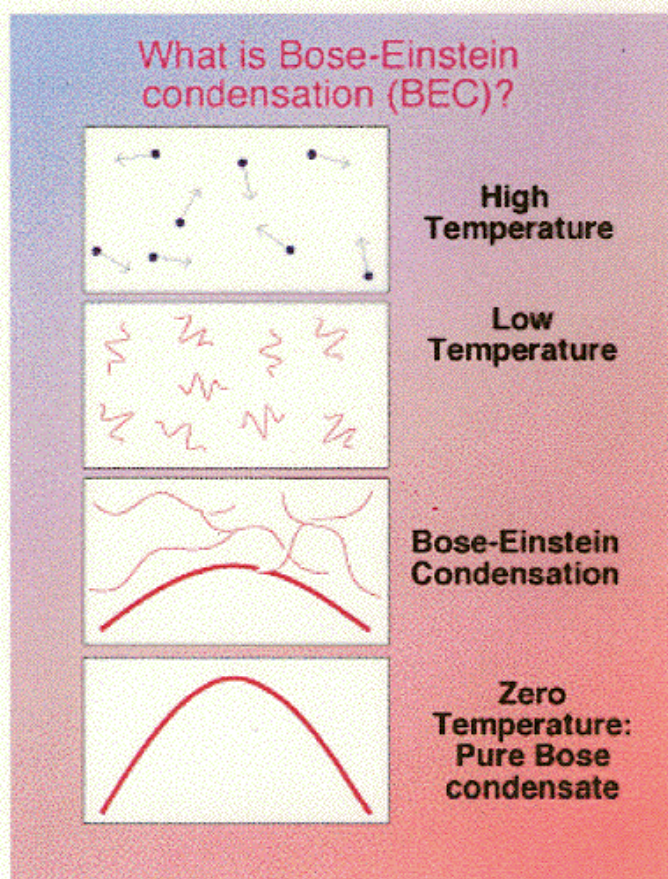
Bose-Einstein condensation (BEC)

At low temperature, the lowest energy state is occupied by the macroscopic number of bosons.

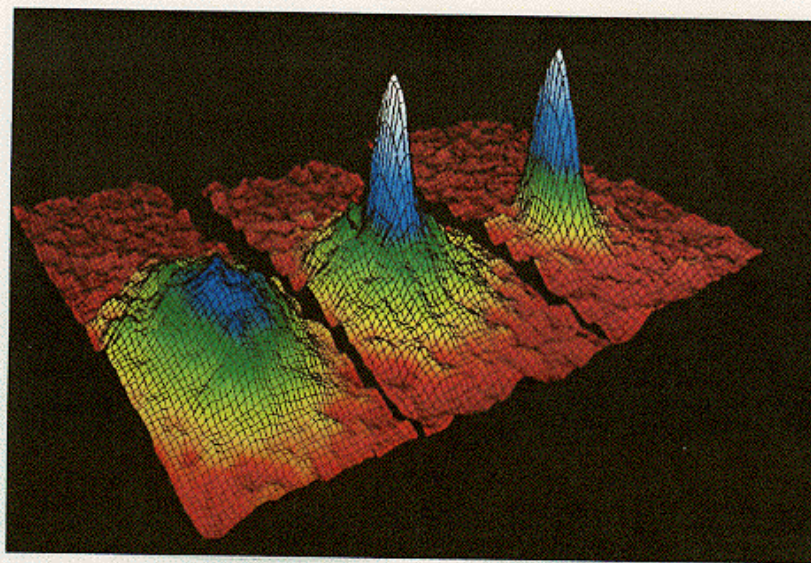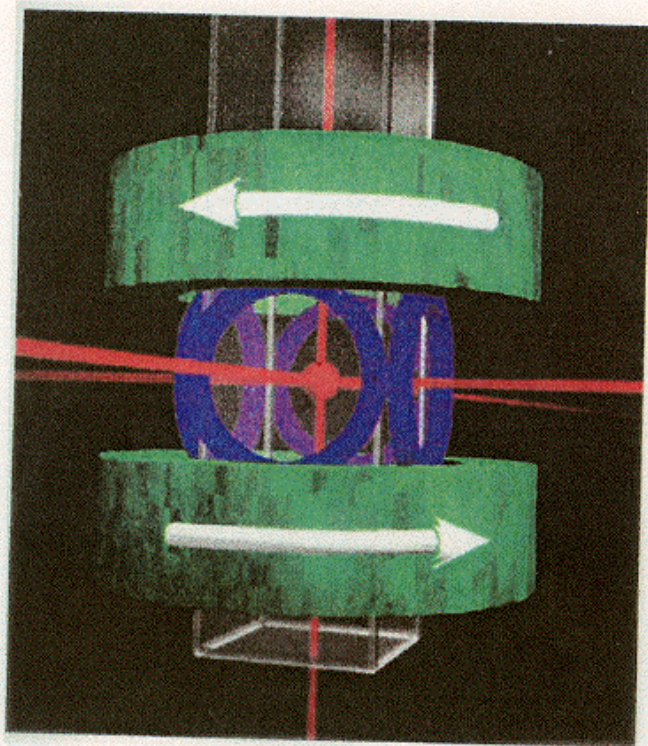thermal de Broglie length $\simeq$ interatomic distance

$$\lambda_{\mathrm{dB}} = \frac{h}{\sqrt{2\pi M k_B T}}$$

What is Bose-Einstein condensation (BEC)?

High Temperature

Low Temperature

Bose-Einstein Condensation

Zero Temperature: Pure Bose condensate

MIT

BEC at JILA

Science **269**, 198 (1995)

BEC of atomic gases

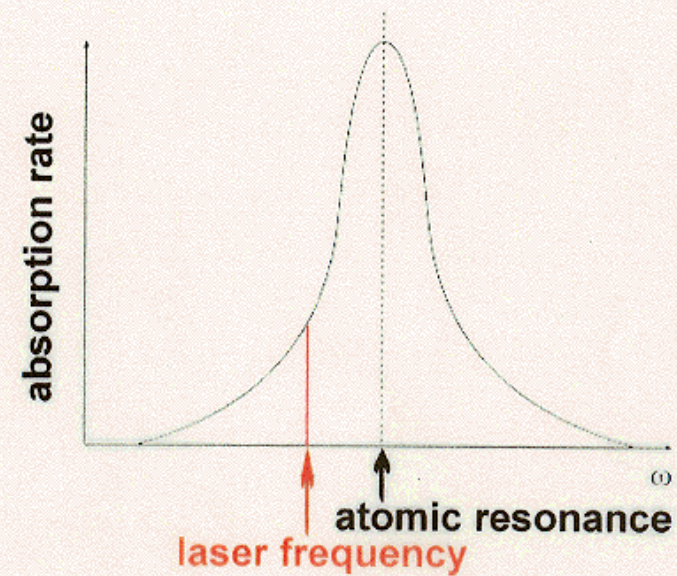| 1995 | ^{87}Rb | — | **JILA** | (Science **269**, 198) |
	^{7}Li	—	**Rice**	(PRL **75**, 1687; **78**, 985)
	^{23}Na	—	**MIT**	(PRL **75**, 3969)
1998	^{1}H	—	**MIT**	(PRL **81**, 3811)
2001	^{85}Rb	—	**JILA**	(PRL **85**, 1795)
	^{4}He*	—	**France**	(Science **292**, 461)
	^{41}K	—	**Firenze**	(Science **294**, 1320)

Laser cooling ($\sim 100\ \mu$K)

$\Downarrow$

Evaporative cooling ($\sim 1\ \mu$K)

$\Downarrow$

BEC

Principle of Laser Cooling

laser   atom   laser

absorption rate

laser frequency   atomic resonance

ω
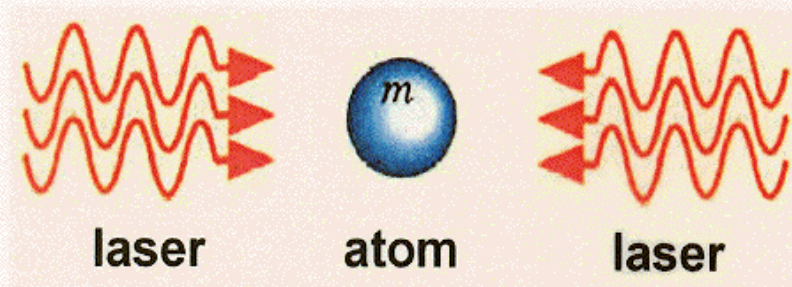
Principle of Evaporative Cooling
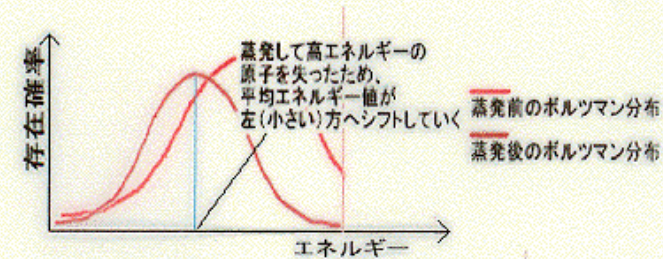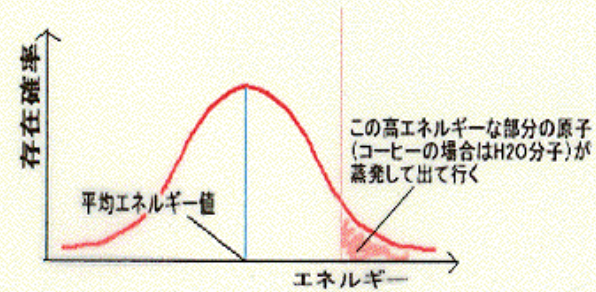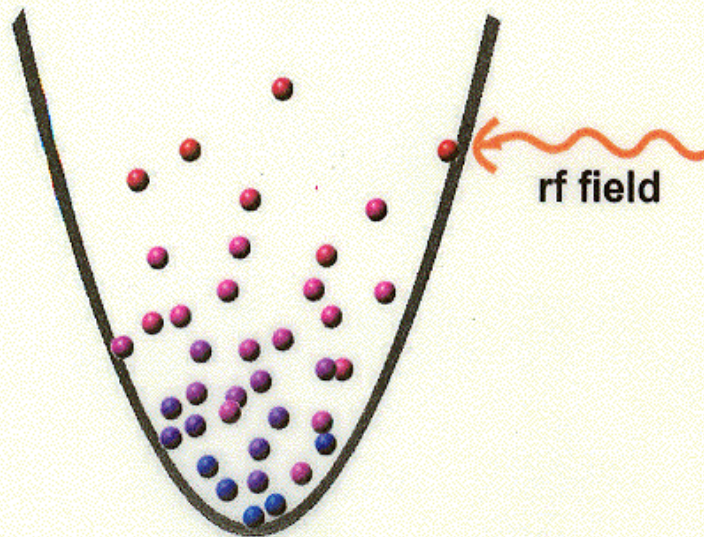
BEC of atomic gases

原子種: ^{87}Rb, ^{23}Na, ^{7}Li, ^{1}H, ^{85}Rb, ^{4}He, ^{41}K

トラップ: 磁気トラップ, 光トラップ

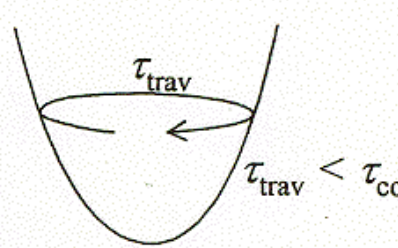温度: μK $\sim$ nK

原子数: $\lesssim 10^7$

原子数密度: $n \sim 10^{14}/\text{cm}^3$

S 波散乱長: $|a| \sim 1$ nm

$$na^3 \sim 10^{-6}$$

	液体ヘリウム	レーザー冷却されたBEC
相	液体→非圧縮性	気体→圧縮性→外部摂動に対する感受率大
BEC	観測は容易でない	容易
超流動性	観測は容易	観測されている
制御性	乏しい	極めて高い (すべてのパラメターが制御可能 非平衡状態の研究に適している)
測定法	中性子散乱	光学的手法(目で見える)
環境(容器、等)のミクロなモデル化	現時点では不可能 (固体表面(容器)の理解が必要)	可能 (但し、まだ理解されていない) →巨視的量子コヒーレンス
運動学 衝突時間 τ_{col} 集団モードの時間スケール ω^{-1}	$\tau_{col} \sim 10^{-12}\text{s} \ll \omega^{-1}$ ↓ ・局所熱平衡状態 ・保存則(エネルギー、連続の式、等)で理解可能	$\tau_{col} \sim 10^{-3}\text{s} \gtrsim \omega^{-1}$ ↓ ・非平衡緩和が本質的 τ_{trav} $\tau_{trav} < \tau_{col}$
内部自由度	(^{3}He の場合)核スピン	(主に)電子スピン ↓ 磁性とBEC

Theory of BEC

Hamiltonian

$$\hat{H} = \int d\mathbf{r}\hat{\psi}^\dagger(\mathbf{r})\left(-\frac{\hbar^2}{2m}\nabla^2 + V_{\text{trap}}(\mathbf{r})\right)\hat{\psi}(\mathbf{r})$$
$$+ \int d\mathbf{r}d\mathbf{r}'\hat{\psi}^\dagger(\mathbf{r})\hat{\psi}^\dagger(\mathbf{r}')U(\mathbf{r}-\mathbf{r}')\hat{\psi}(\mathbf{r}')\hat{\psi}(\mathbf{r})$$

interaction

$$U(\mathbf{r}-\mathbf{r}') = \frac{4\pi\hbar^2 a}{m}\delta(\mathbf{r}-\mathbf{r}') \qquad a : \text{s-wave scattering length}$$

trap potential

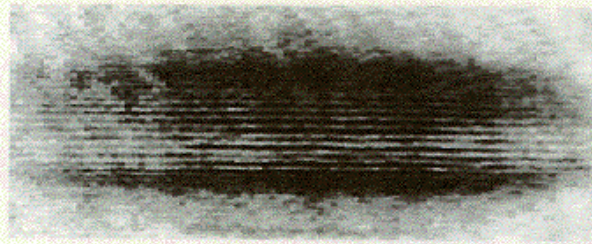$$V_{\text{trap}}(\mathbf{r}) = \frac{m}{2}[\omega_\perp^2(x^2+y^2) + \omega_z^2 z^2]$$

Gross-Pitaevskii equation (mean-field approx.)

$$i\hbar\frac{\partial\psi}{\partial t} = \left[-\frac{\hbar^2}{2m}\nabla^2 + V_{\text{trap}}(\mathbf{r})\right]\psi + \frac{4\pi\hbar^2 a}{m}|\psi|^2\psi$$

BEC experiments

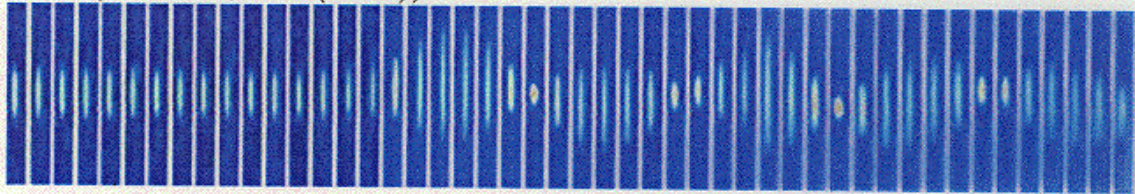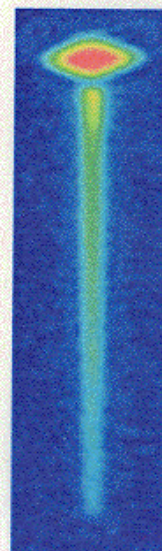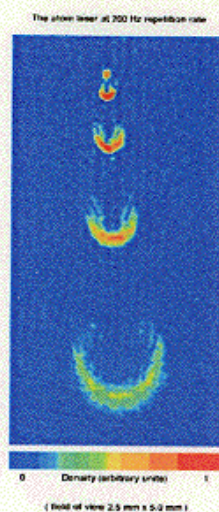- ## Interference between two BECs

  MIT (Science **275**, 637 (1997))

- ## Collective excitation

  MIT (PRL **81**, 500 (1998))

- ## Atom laser

  MIT (PRL **78**, 582 (1997))   Max Planck (PRL **82**, 3008 (1999))

Bosonic Stimulation in the Formation of a Bose-Einstein Condensate

H.-J. Miesner, D. M. Stamper-Kurn, M. R. Andrews,
D. S. Durfee, S. Inouye, W. Ketterle

rf sweep 10 ms   13 ms per frame
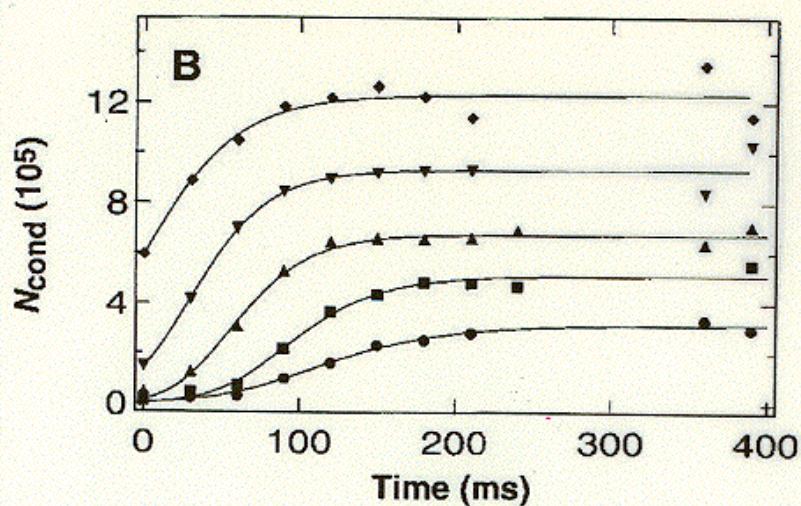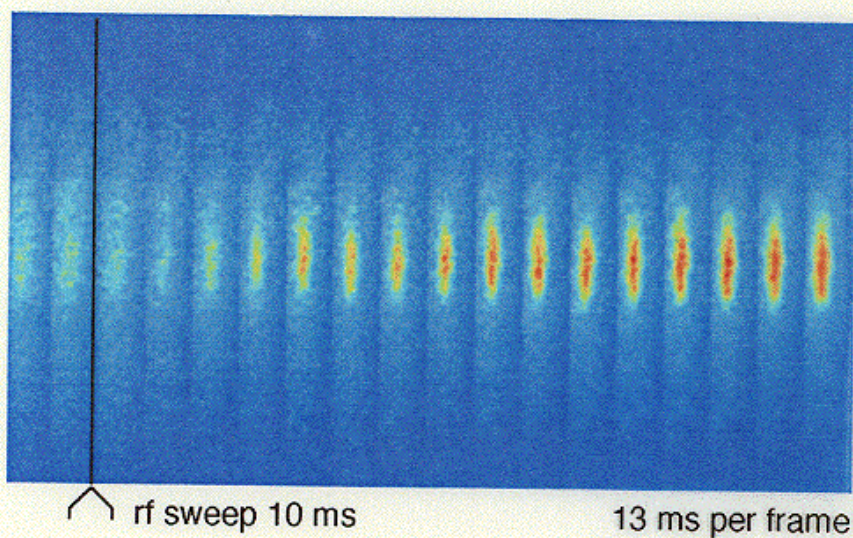
$$\dot{N_o} = \gamma N_o \left[1 - \left(\frac{N_o}{N_{o.eq}} \right)^{5/2} \right]$$

C. Gardiner et al. PRL 79 1793 (1997)
                    PRL 81 5266 (1998)

....

Measurement of the spatial coherence of a trapped Bose gas at the phase transition

I. Bloch, T. W. Hänsch & T. Esslinger

Sektion Physik, Ludwig-Maximilians-Universität, Schellingstrasse 4/III, D-80799 Munich, Germany, & The Max-Planck-Institut für Quantenoptik, D-85748 Garching, Germany

....
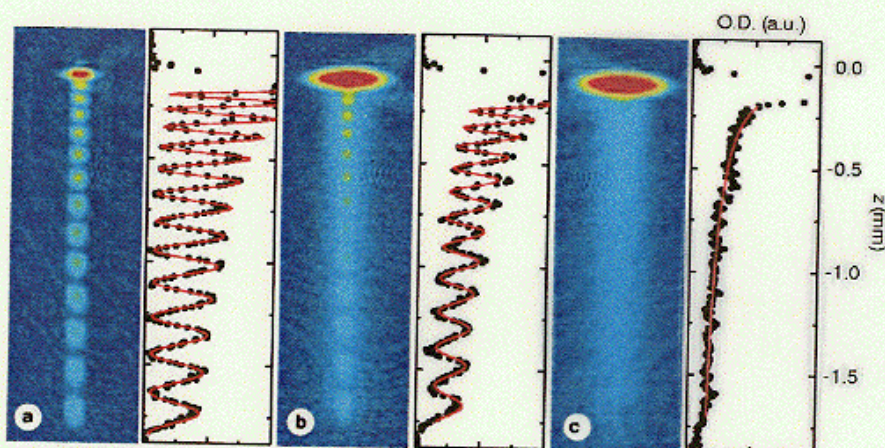

Figure 1 Interference pattern of matter-wave beams emitted from two spatially separated regions of a trapped Bose gas. **a–c**, The absorption images show the spatial distribution of the output beams for three different temperatures in false colours. For a temperature well below the critical temperature T_c the spatially uniform phase of the condensate results in a high-contrast interference pattern (**a**). When the temperature is increased to just below T_c the contrast of the interference pattern is reduced (**b**), and it vanishes completely for temperatures above T_c (**c**). Each of the images has a size of 0.6 mm × 2 mm. The frequency difference between the two components of the radio-wave field was 1,000 Hz, which corresponds to a slit separation of 465 nm. The plots next to the images show 21-μm-wide vertical cuts through the centres of the absorption images. The horizontal axes of the plots show the optical densities. We obtain the visibilities V by using equation (1) to fit the data.
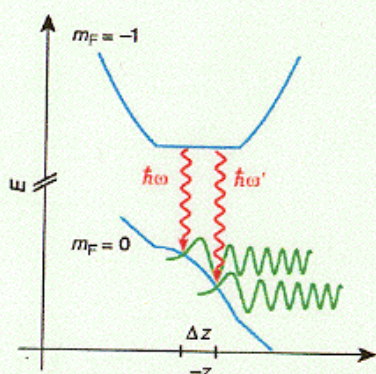

Figure 2 Measurement of the spatial coherence of a trapped Bose–Einstein condensate. A radio-wave field with two frequency components (red lines) transfers magnetically trapped atoms ($m_F = -1$) into untrapped states ($m_F = 0$). Two matter wave beams (green lines) are emitted from spatially separated locations in the trap, thereby effectively forming a double slit. The beams are accelerated by gravity and overlap outside the trap so that an interference pattern can be observed. A high contrast is detected if the trapped gas is spatially coherent over both slit regions. The harmonic potential for the trapped state and the linear potential for the untrapped state are modified by the mean field of the condensate (blue lines).
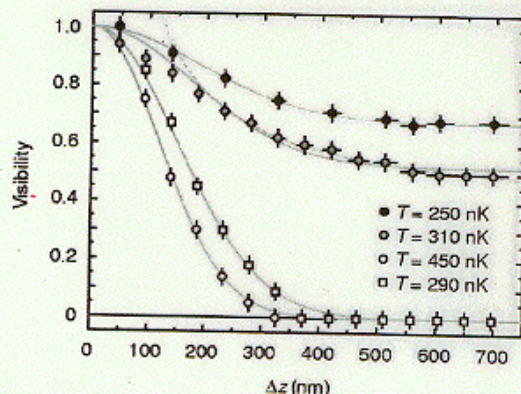

Figure 4 Spatial correlation function of a trapped Bose gas. The fringe visibility is measured as a function of slit separation for temperatures above and below the critical temperature T_c. The white circles and white squares show the measurements for thermal gases at temperatures of 450 nK and 290 nK, respectively. (To prepare a thermal gas at a temperature of 290 nK we reduced the number of atoms in the trap to 10^6). The grey data points (310 nK) and the black data points (250 nK) are the results obtained for temperatures below T_c, where the visibility decays to a nonzero value due to the long-range phase coherence of the condensate fraction. The decay of the visibility shows a longer tail than would be expected for the corresponding de Broglie wavelength of the thermal fraction. Both data sets are fitted with a gaussian function and an offset. For the temperature of 310 nK the last 11 data points are also fitted with a function proportional to

BEC in the Microtrap
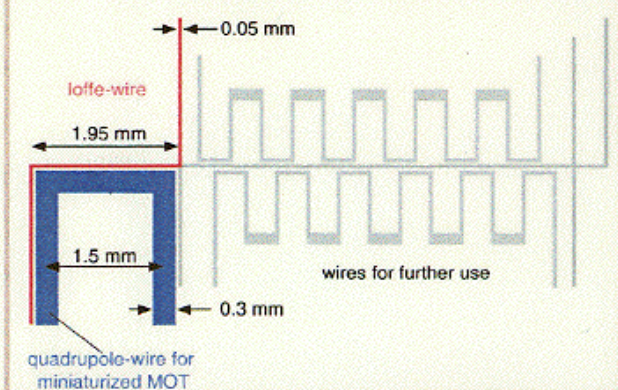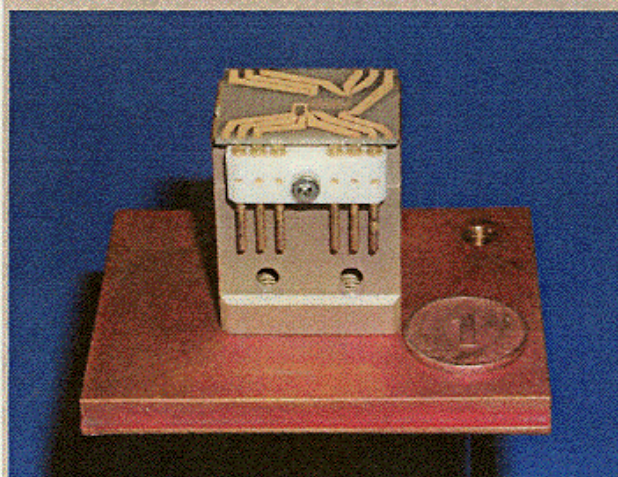## MPQ Magnetic Microtrap Project

On 12 June 2001,
a Bose-Einstein condensate of ^{87}Rb atoms
was born in a microtrap.
(Atoms are trapped in the $|F=2, m_F=2>$-state)

absorption images after 20 ms of free expansion

(the small cloud to the right of the main condensate stems from atoms
that undergo a spin-flip to the $m_F=1$ state when the magnetic field is shut off)

loffe-wire
0.05 mm
1.95 mm
1.5 mm
0.3 mm
wires for further use
quadrupole-wire for
miniaturized MOT

The Way to Bose-Einstein Condensation in a Magnetic Microtrap

MOT 1	MOT with external quadrupole coils: we load 6×10^6 atoms within 8 s.
MOT 2	MOT with miniaturized quadrupole field: ~1 A in the quadrupole wire (blue) + homogeneous magnetic field of 3 G
Microtrap 1	Transfer 3×10^6 atoms into the magnetic trap: 2A in the Ioffe-wire (red) + homogeneous field of 8 G.
Microtrap	Compress the magnetic trap

Bose–Einstein condensation on a microelectronic chip

W. Hänsel, P. Hommelhoff, T. W. Hänsch & J. Reichel

*Max-Planck-Institut für Quantenoptik and Sektion Physik der
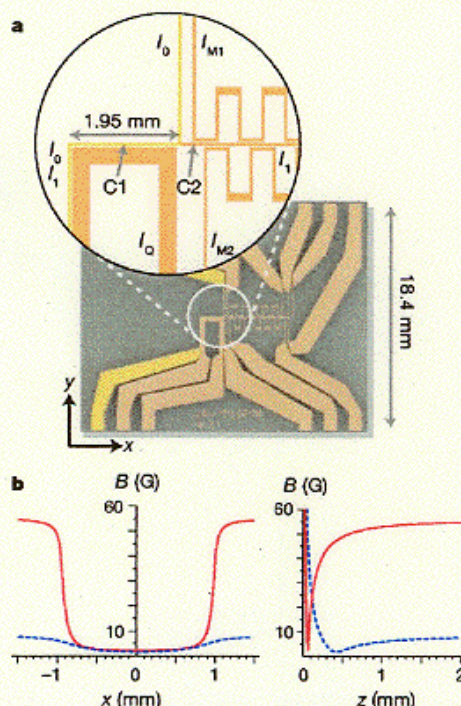Ludwig-Maximilians-Universität, Schellingstr. 4, D-80799 München, Germany*

Figure 1 The chip and the magnetic potentials that it creates. **a**, Layout of the lithographic gold wires on the substrate. The inset shows the relevant part of the conductor pattern. I_0, I_1, I_{M1} and I_{M2} create the various magnetic potentials for trapping (see **b**) and transport, as described in the main text. I_Q is used only during trap loading (intermediate MOT step[5]). **b**, Potentials created by a wire current $I_0 = 2$ A for two different values of the external bias field, ($B_x = 0$, $B_y = 8$ G) (dashed lines) and ($B_x = 1.9$ G, $B_y = 55$ G) (solid lines).
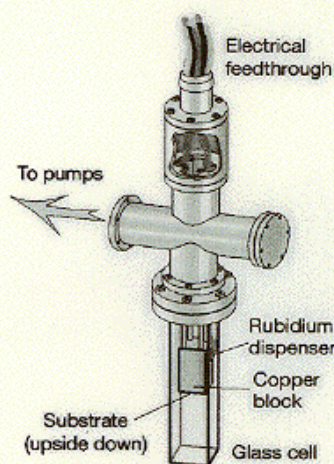

Figure 2 Vacuum system. Because of the efficient evaporation in the chip trap, this very simple set-up is sufficient to achieve Bose–Einstein condensation (BEC). The substrate is mounted facing downwards, so that the atom cloud may be released to expand in free fall (time-of-flight analysis).
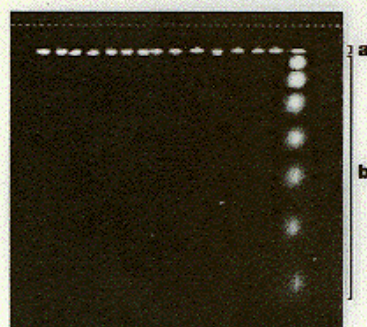

Figure 5 Transport of a BEC on the 'magnetic conveyor belt'. **a**, Superposed absorption images taken at fixed time intervals during transport. The distance between the first and last image is 1.6 mm, the transport time is 100 ms. The line of sight is parallel to the *y* axis (see Fig. 1); the dotted line marks the edge of the substrate. **b**, Time-of-flight images of the atom cloud after release at the final position, exhibiting the bimodal structure characteristic of a BEC. The maximum expansion time (bottom image) is 19.3 ms.
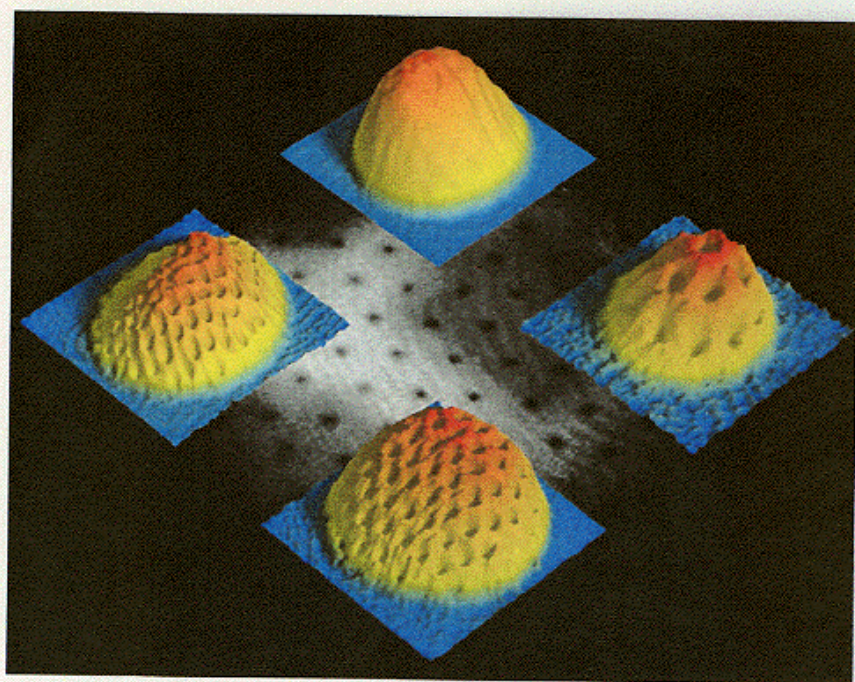
ENS ^{87}Rb

$\Omega < \Omega_c$

$\Omega > \Omega_c$
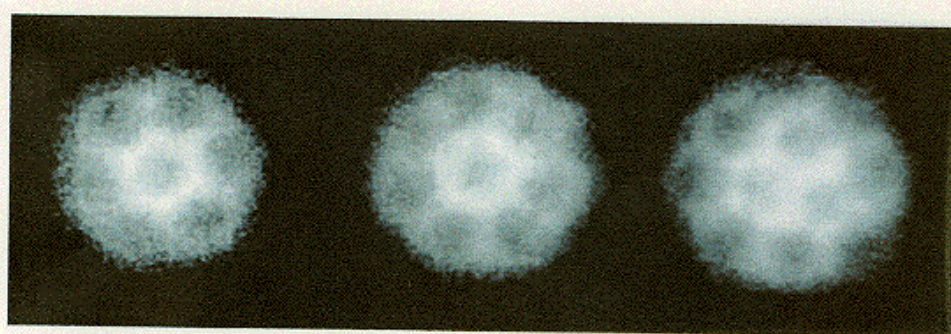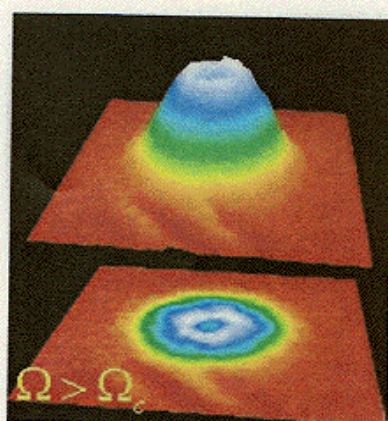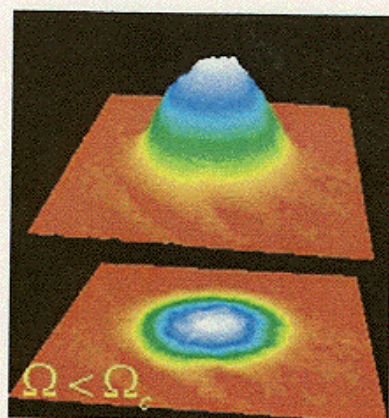
MIT ^{23}Na

Observation of Vortex Lattices
in Bose-Einstein Condensates

J. R. Abo-Shaeer, C. Raman, J. M. Vogels, W. Ketterle

g. 4. Formation and cay of a vortex lat- e. The condensate s rotated for 400 ms d then equilibrated the stationary mag- tic trap for various ld times. (A) 25 ms, 100 ms, (C) 200 ms, 500 ms, (E) 1 s, (F) s, (G) 10 s, and (H) s. The decreasing e of the cloud in (E) (H) reflects a de- ase in atom number e to inelastic colli- ns. The field of view ~1 mm by 1.15 mm.
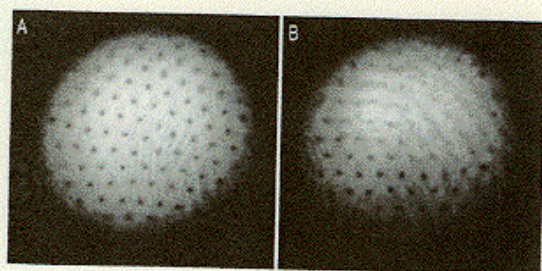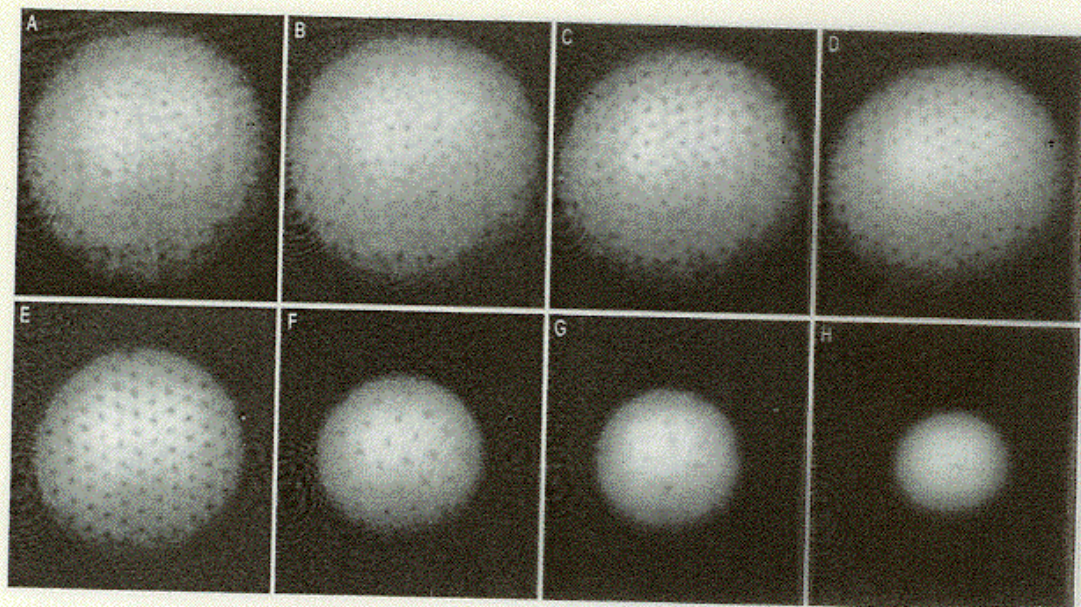

Fig. 5. Vortex lattices with de- fects. In (A), the lattice has a dislocation near the center of the condensate. In (B), there is a defect reminiscent of a grain boundary.
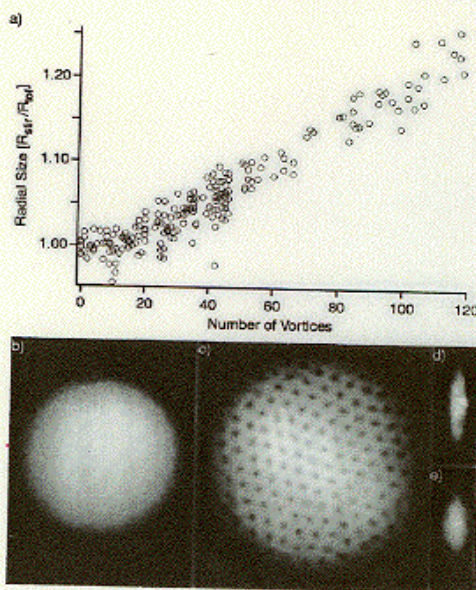
FIG. 4. Centrifugal effects on a rotating condensate. Shown is the observed radial size of the condensate versus vortex number. The condensate size was determined from a parabolic fit to the time-of-flight distribution after 41.5 ms. (b,c) Comparison of a non-rotating condensate ($R_{tof} = 570$ μm) and one with 160 vortices. Radial in-situ phase contrast imaging of a condensate at rest (d) and in rotation at a fre- quency of 75 Hz (e), showing the modified aspect ratio. The length of the condensate in (d) was 200 μm.

Observation of Fermi Pressure
in a Gas of Trapped Atoms

Andrew G. Truscott, Kevin E. Strecker, William I. McAlexander,*
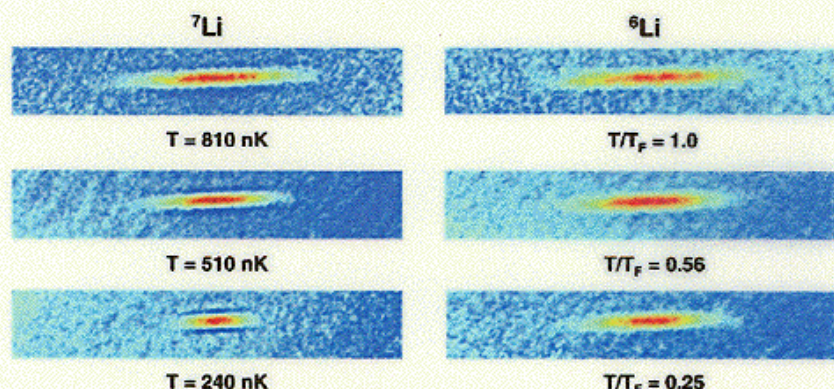Guthrie B. Partridge, Randall G. Hulet†

Fig. 1. Two-dimensional false-color images of both ^{7}Li and ^{6}Li clouds. At $T/T_F = 1.0$, the two clouds are approximately the same size, but as the atoms are cooled further, to $T/T_F = 0.56$, the Bose gas contracts, whereas the Fermi gas exhibits only subtle changes in size. At $T/T_F = 0.25$, the size difference between the two gases is clearly discernable. At this temperature the ^{7}Li image displays distortions due to high optical density. However, these distortions are present only in the radial direction and do not affect the measurements. The fitted numbers of ^{7}Li and ^{6}Li atoms, N_7 and N_6, and the fitted temperatures are as follows: For the upper set, $N_7 = 2.4 \times 10^5$, $N_6 = 8.7 \times 10^4$, and $T = 810$ nK; for the middle set, $N_7 = 1.7 \times 10^5$, $N_6 = 1.3 \times 10^5$, and $T = 510$ nK; and for the lower set, $N_7 = 2.2 \times 10^4$, $N_6 = 1.4 \times 10^5$, and $T = 240$ nK. The probe detuning is a parameter of the fits but is constrained to vary by no more than its uncertainty of ± 3 MHz. The fits result in typical reduced-χ^2 values of ~1.0. The uncertainties in number and temperature are due mainly to the uncertainties in the fit and are roughly estimated by finding the point at which the reduced-χ^2 increases by 20%. The resulting uncertainties are 8% in temperature and 15% in number. Other sources of uncertainty are relatively insignificant. The size of each displayed image is 1.00 mm in the horizontal axis and 0.17 mm in the vertical axis.
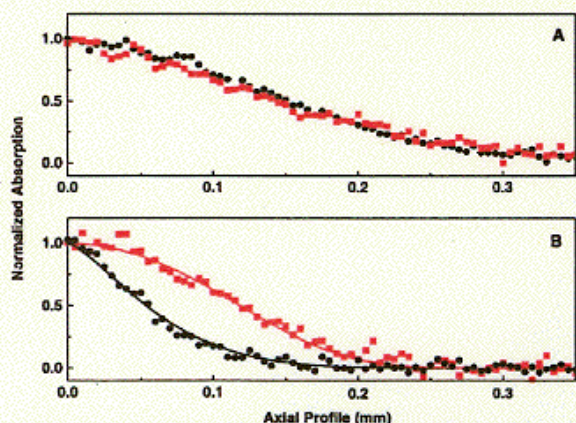

Fig. 3. Square of the 1/e axial radius, r, of the ^{6}Li clouds versus T/T_F. The radius is normalized by the Fermi radius, $R_r = (2k_BT_F/m\omega_r^2)^{1/2}$, where m is the atomic mass of ^{6}Li. The solid line is the prediction for an ideal Fermi gas, whereas the dashed line is calculated assuming classical statistics. The data are shown as open circles. The divergence of the data from the classical prediction is the result of Fermi pressure. Several representative error bars are shown. These result from the uncertainties in number and temperature as described in the legend to Fig. 1. In addition, we estimate an uncertainty of 3% in the determination of r.

Fig. 2. Comparison of ^{6}Li and ^{7}Li atom cloud axial profiles. The red squares correspond to ^{6}Li, and the black circles to ^{7}Li. (A) Data from the top image of Fig. 1, corresponding to $T/T_F = 1.0$ and $T/T_c = 1.5$. (B) Data from the lower image of Fig. 1, corresponding to $T/T_F = 0.25$ and $T/T_c = 1.0$. The fits to the data are shown as solid lines.
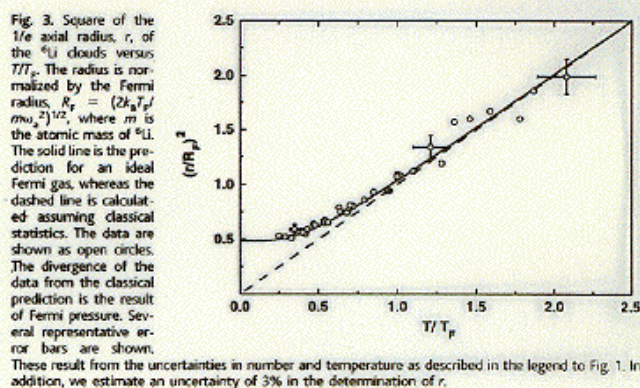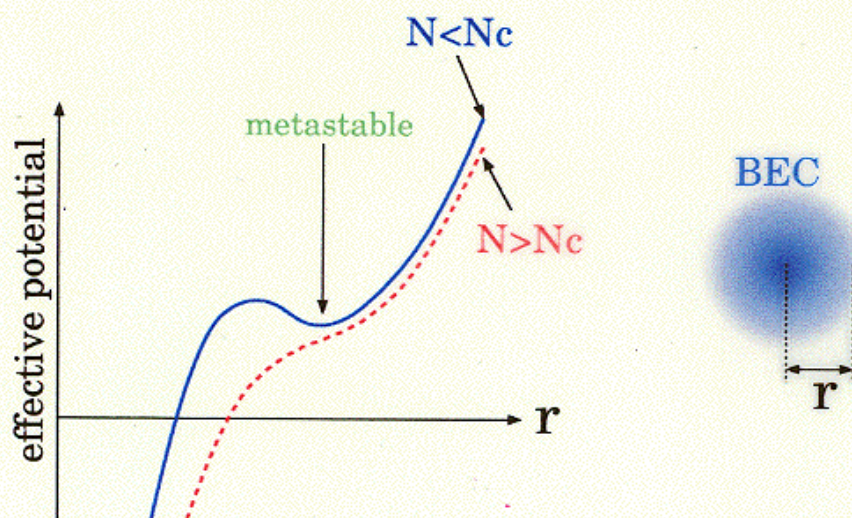
BEC with attractive interactions

^{7}Li, ^{85}Rb —— attractive interaction

Attractive BEC can be metastable.

$$\begin{cases} \text{Kinetic energy} & \propto r^{-2} \\ \text{Potential energy} & \propto r^2 \\ \text{Interaction energy} & \propto -r^{-3} \end{cases}$$

$$\frac{N|a|}{a_{\text{ho}}} \quad < \quad 0.57 \quad \text{(theory)}$$

$$\lesssim \quad 0.46 \quad \text{(experiment)}$$

J. L. Roberts *et al.*, **PRL 86, 4211 (2001)**

···

Direct observation of growth and collapse of a Bose–Einstein condensate with attractive interactions

Jordan M. Gerton*, **Dmitry Strekalov***†, **Ionut Prodan*** **& Randall G. Hulet***
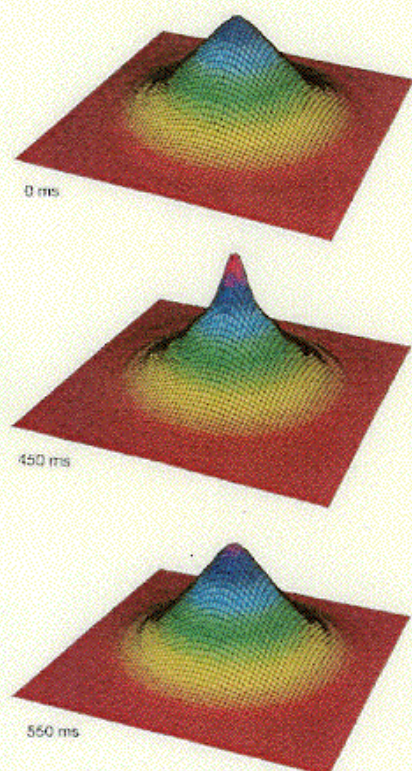
Figure 4 Phase-contrast images. These images were selected from those used to construct Fig. 3a. The upper image corresponds to data immediately after the dump pulse (0 ms), the middle image to the peak of condensate growth (450 ms), and the lower image to the first collapse (550 ms). The fitted values of N_0 are 40, 1,210 and 230 atoms for the upper, middle and lower images, respectively. The displayed images result from angle-averaging the actual images about the probe laser propagation axis and the signal height is proportional to the column density of the atom cloud integrated along this direction[4]. The image area corresponds to a square of sides 85 μm. A movie of the growth and collapse was produced using representative time-ordered images from the data of Fig. 3a, and is available for viewing at http://atomcool.rice.edu/collapse.html.
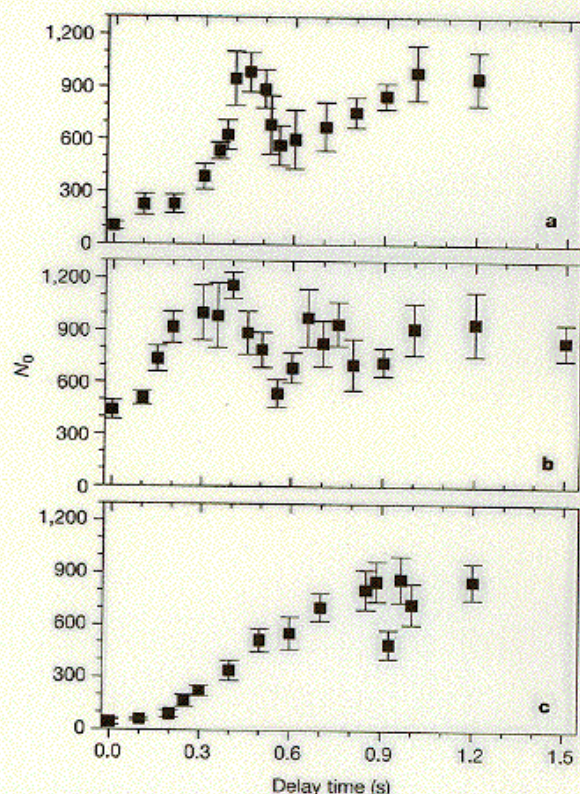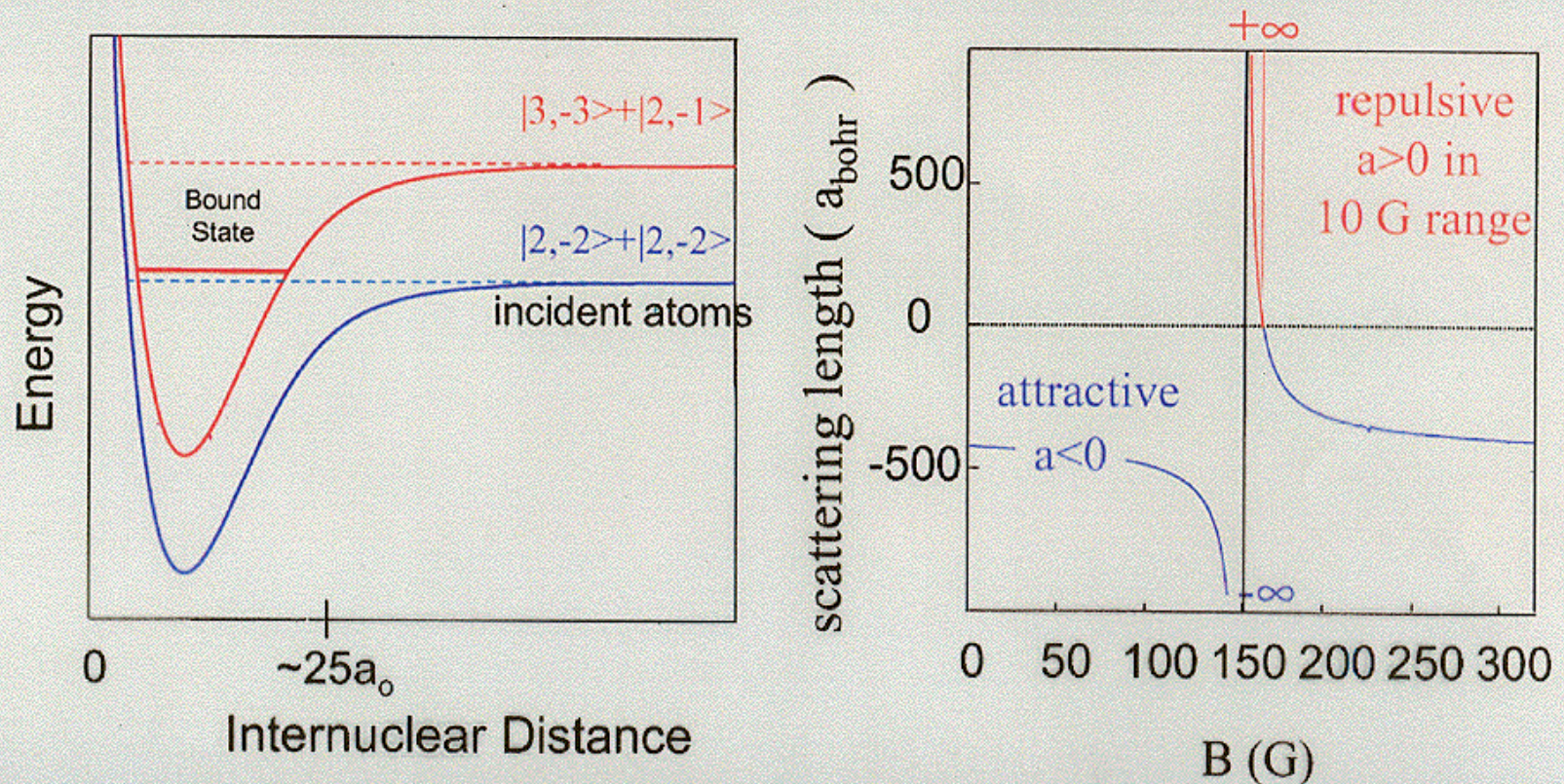

Figure 3 Condensate growth and collapse dynamics. Each data point is the mean of five measurements for the same delay time following the light pulse, and the error bars are the standard deviation of the mean. **a**, N_0 is reduced to ~100 atoms using the two-photon light pulse. The reduction in N_0 after the first peak at 450 ms is a direct manifestation of collapse. **b**, The condensate is only partially dumped in order to speed up the initial growth. Subsequent maxima and minima are observed as the gas continues to undergo growth and collapse cycles while evolving towards thermal equilibrium. **c**, The light pulse duration is increased, so that the condensate is dumped completely, to within the experimental resolution. We note the slow turn-on of growth and the subsequent saturation in the growth rate (see text). For **a** and **c**, there is a 3-s delay following the microwave quench pulse before the light pulse; whereas in **b**, the delay is 5 s. Additionally, for **a** and **c**, $N = (7 \pm 1) \times 10^4$ atoms and $T = (170 \pm 15)$ nK immediately before the light pulse, while for **b**, $N = (1.0 \pm 0.1) \times 10^5$ atoms and $T = (200 \pm 20)$ nK. For each individual image, the statistical uncertainty in N_0 is ±60 atoms, while the systematic uncertainty, dominated by uncertainties in the imaging system, is ±20%[13].

Feshbach Resonance in Ultracold Atom Collisions

Can adjust a !

Left panel — Energy vs. Internuclear Distance:
- $|3,-3>+|2,-1>$
- Bound State
- $|2,-2>+|2,-2>$
- incident atoms
- 0
- $\sim 25a_o$
- Internuclear Distance

Right panel — scattering length (a_{bohr}) vs. B (G):
- $+\infty$
- 500
- repulsive $a>0$ in 10 G range
- 0
- attractive $a<0$
- -500
- $-\infty$
- 0 50 100 150 200 250 300
- B (G)

Since a can be adjusted, the condensate mean-field energy can be tuned to any desired value.

Stable ^{85}Rb Bose-Einstein Condensates with Widely Tunable Interactions

S. L. Cornish, N. R. Claussen, J. L. Roberts, E. A. Cornell,* and C. E. Wieman

JILA, National Institute of Standards and Technology, and the Department of Physics, University of Colorado, Boulder, Colorado 80309-0440

Bose-Einstein condensation has been achieved in a magnetically trapped sample of ^{85}Rb atoms. Long-lived condensates of up to 10^4 atoms have been produced by using a magnetic-field-induced Feshbach resonance to reverse the sign of the scattering length. This system provides new opportunities for the study of condensate physics. The variation of the scattering length near the resonance has been used to magnetically tune the condensate self-interaction energy over a wide range, extending from strong repulsive to large attractive interactions. When the interactions were switched from repulsive to attractive, the condensate shrank to below our resolution limit, and after ~5 ms emitted a burst of high-energy atoms.
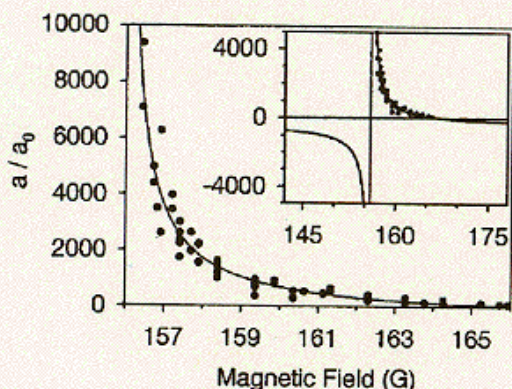
PRL 85 1795 (2000)

FIG. 1.   Scattering length in units of the Bohr radius (a_0) as a function of the magnetic field. The data are derived from the condensate widths. The solid line illustrates the expected shape of the Feshbach resonance using a peak position and resonance width consistent with our previous measurements [4,18]. For reference, the shape of the full resonance has been included in the inset.
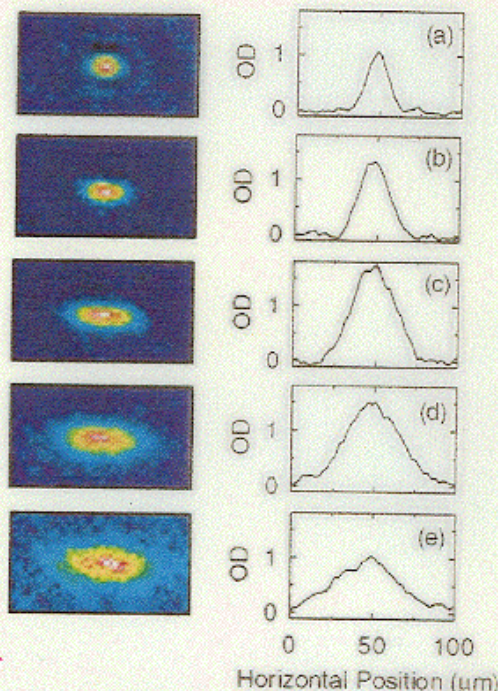

FIG. 3 (color).   False color images and horizontal cross sections of the condensate column density for various magnetic fields. The condensate number was varied to maintain an optical depth (OD) of ~1.5. The magnetic field values are (a) $B = 165.2$ G, (b) $B = 162.3$ G, (c) $B = 158.4$ G, (d) $B = 157.2$ G, and (e) $B = 156.4$ G.

Dynamics of collapsing and exploding Bose–Einstein condensates

Elizabeth A. Donley*, Neil R. Claussen*, Simon L. Cornish*, Jacob L. Roberts*, Eric A. Cornell*† & Carl E. Wieman*

* JILA, Campus Box 440, and Department of Physics, Campus Box 390, University of Colorado, Boulder, Colorado 80309, USA
† Quantum Physics Division, National Institute of Standards and Technology, JILA A231, Boulder, Colorado 80309, USA
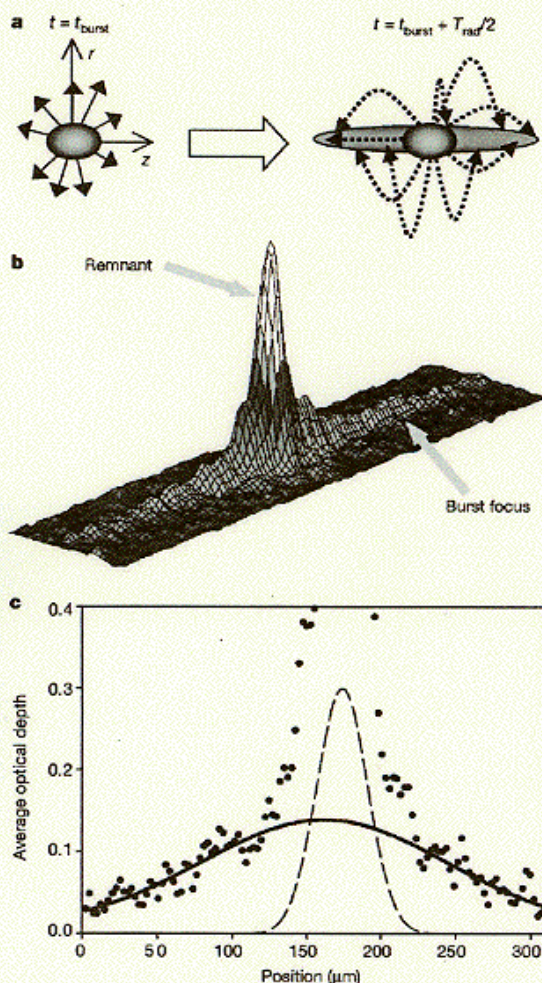
Pre-Collapse Condensate

Post-Collapse Remnant
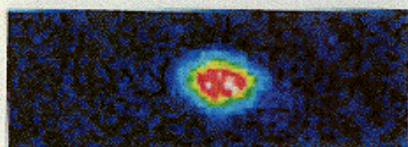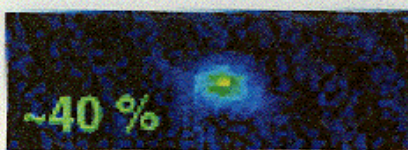
~40 %

Burst of "Hot" Atoms

~30 %

Figure 3 A burst focus. **a**, Conceptual illustration of a radial burst focus. t_{burst} is the time at which the burst is generated and T_{rad} is the radial trap period. **b**, An image of a radial burst focus taken 33.5 ms after a jump from $a_{init} = 0$ to $-30a_0$ for $N_0 = 10,000$. $T_{rad}/2 = 28.6$ ms, which indicates that the burst occurred 4.9(5) ms after the jump. The axial energy distribution for this burst corresponded to an effective temperature of 62 nK. The image is 60×310 μm. **c**, Radially averaged cross-section of **b** with a gaussian fit to the burst energy distribution. The central 100 μm were excluded from the fit to avoid distortion in the fit due to the condensate remnant ($\sigma = 9$ μm) and the thermal cloud ($\sigma = 17$ μm). The latter is present in the pre-collapse sample due to the finite temperature, and appears to be unaffected by the collapse. The dashed line indicates the fit to this initial thermal component. We note the offset between the centres of the burst and the remnant. This offset varies from shot to shot by an amount comparable to the offset shown.
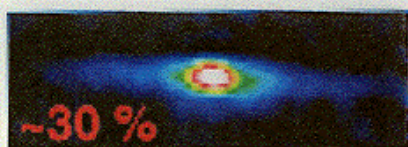
BEC → Remnant
→ Burst
→ Missing

Dynamics of collapsing and exploding Bose–Einstein condensates

Elizabeth A. Donley*, Neil R. Claussen*, Simon L. Cornish*, Jacob L. Roberts*, Eric A. Cornell*† & Carl E. Wieman*

* JILA, Campus Box 440, and Department of Physics, Campus Box 390, University of Colorado, Boulder, Colorado 80309, USA
† Quantum Physics Division, National Institute of Standards and Technology, JILA A231, Boulder, Colorado 80309, USA
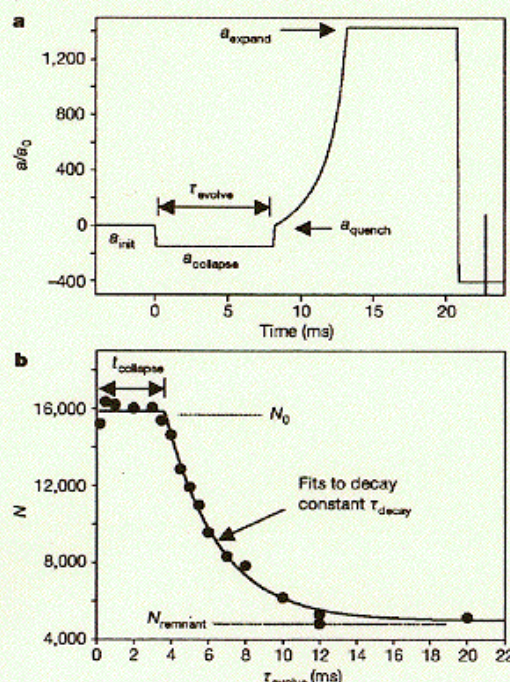
"jets"

Figure 1 An example of a ramp applied to the scattering length a, and a plot of the condensate number N versus time after a jump to a negative scattering length. **a**, A typical $a(t)$ sequence. $a_0 = 0.529$ Å is the Bohr radius. The scattering length is jumped at $t = 0$ in 0.1 ms from a_{init} to $a_{collapse}$, where the BEC evolves for a time τ_{evolve}. The field is carefully controlled so that magnetic-field noise translates into fluctuations in $a_{collapse}$ on the order of $\sim 0.1a_0$ in magnitude. The collapse is then interrupted with a jump to a_{quench}, and the field is ramped in 5 ms to a large positive scattering length which makes the BEC expand. After 7.5 ms of additional expansion, the trap is turned off in 0.1 ms, and 1.8 ms later the density distribution is probed using destructive absorption imaging with a 40-μs laser pulse (indicated by the vertical bar). The increase in a from $a_{collapse}$ to a_{expand} is far too rapid to allow for the BEC to expand adiabatically. On the contrary, the smaller the BEC before expansion, the larger the cloud at the moment of imaging. Thus we can readily infer the relative size of the bulk of the BEC just before the jump to a_{quench}. The density of the expanded BEC is so low that the rapid transit of the Feshbach resonance pole[25] during the trap turn-off and the subsequent time spent at magnetic field $B = 0$ ($a = -400a_0$) both have a negligible effect. **b**, The number of atoms remaining in the BEC versus τ_{evolve} at $a_{collapse} = -30a_0$. We observed a delayed and abrupt onset of loss. The solid line is a fit to an exponential with a best-fit value of $t_{collapse} \approx 3.7(5)$ ms for the delay.
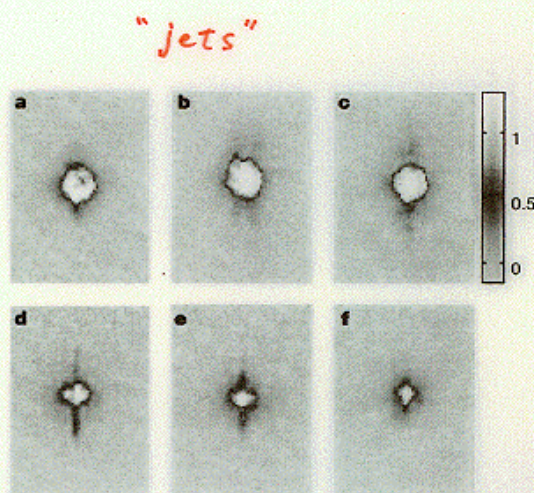
Figure 5 Jet images for a series of τ_{evolve} values for the conditions of Fig. 1b. The evolution times were 2, 3, 4, 6, 8 and 10 ms (from **a** to **f**). Each image is 150×255 μm. The bar indicates the optical depth scale. An expansion to $a_{expand} = +250a_0$ was applied, so the jets are longer than for the quantitative measurements explained in the text. The jets were longest (that is, most energetic) and contained the most atoms at values of τ_{evolve} for which the slope of the loss curve (Fig. 1b) was greatest. A tiny jet is barely visible for $\tau_{evolve} \approx 2$ ms (**a**), which is 1.7 ms before $t_{collapse}$. The images also show how the number of condensate atoms decreases with time. The time from the application of a_{quench} until the acquisition of the images was fixed at 5.2 ms.
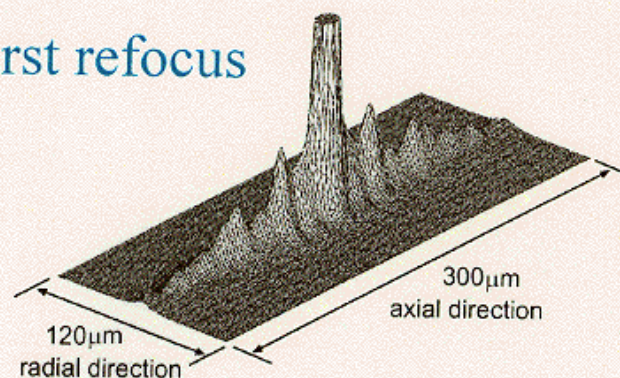
Results of our simulations

H. Saito and M. Ueda, PRL **86**, 1406 (2001); PRA **63**, 043601 (2001); cond-mat/0107248
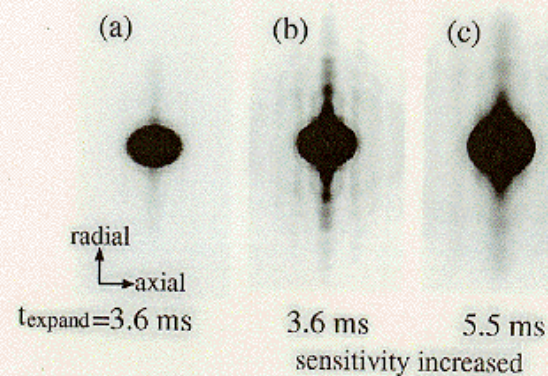
Condensate decay
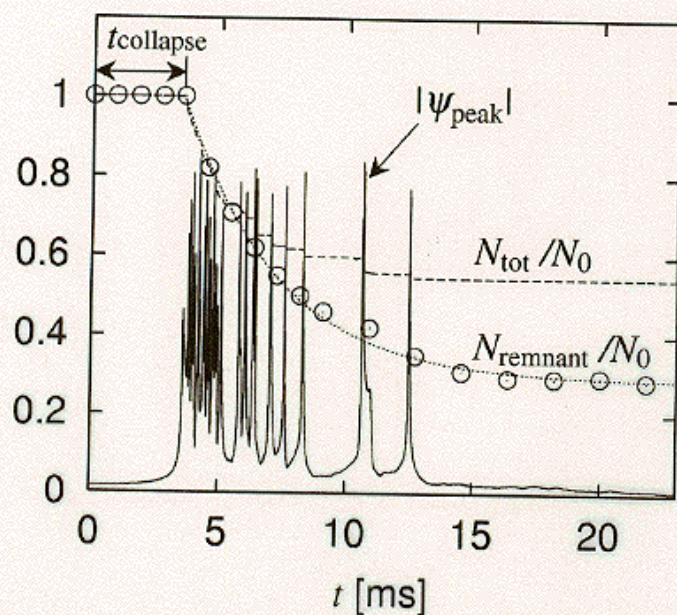
Burst refocus

Jet formation

今後の展望

- 原子間相互作用の変化
  希薄BEC → 液体He → ？
  引力BECの性質

- 量子情報への応用
  entangled 状態の生成

- 超精密測定への応用

参考文献 (レビュー、解説記事)

- 実験

  ◇ E. A. Cornell *et al.*, cond-mat/9903109

  ◇ W. Ketterle *et al.*, cond-mat/9904034, 0005001, 0101424

- 理論

  ◇ F. Dalfovo *et al.*, Rev. Mod. Phys. <u>71</u>, 463 (1999)

  ◇ A. J. Leggett, Rev. Mod. Phys. <u>73</u>, 307 (2001)

  ◇ Y. Castin, cond-mat/0105058

- 解説記事

  ◇ 上田正仁, 日本物理学会誌 <u>53</u>, 663 (1998)

  ◇ 久我隆弘, 日本物理学会誌 <u>55</u>, 90 (2000)

  ◇ パリティ, 1999 年 9 月号

  ◇ 鶴見剛也, 和達三樹, 科学 <u>69</u>, 937 (1999)

  ◇ 斎藤弘樹, 上田正仁, 固体物理 <u>36</u>, 311 (2001)

- Web ページ

  ◇ http://bec01.phy.gasou.edu/bec.html

Physical interpretation of intermittent implosion

The atoms rapidly accumulate at the center of the trap due to the attractive interaction.

When the central density becomes large, the three-body recombination loss dominates.

The loss of atoms decreases the centripetal force, and the atoms are ejected outwards due to the uncertainty principle.

The inward flow of the atoms again replenishes the central density.
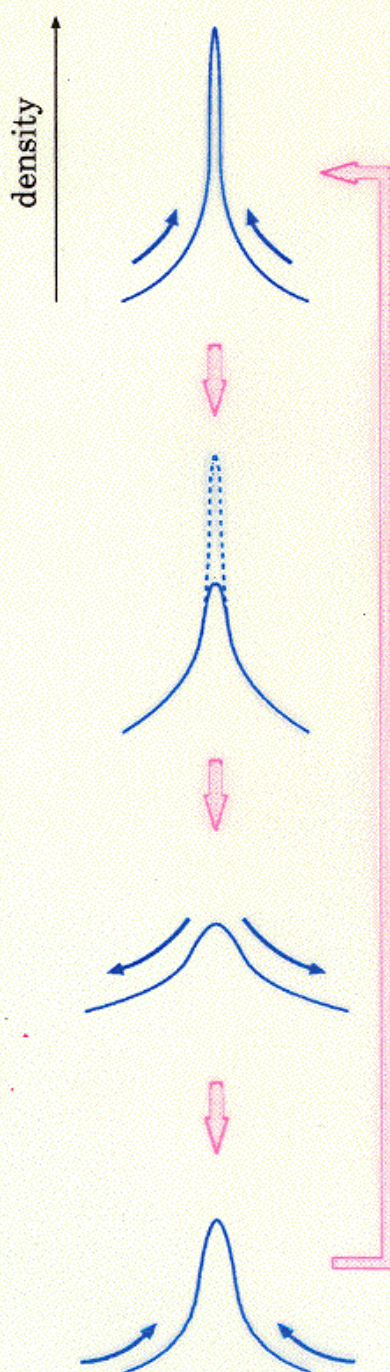
The Gross-Pitaevskii equation with losses

The mean-field approximation is applicable.

Gross-Pitaevskii equation with losses

$$i\hbar\frac{\partial\psi}{\partial t} = \left[-\frac{\hbar^2}{2m}\nabla^2 + V_{\text{trap}}(\mathbf{r})\right]\psi + \frac{4\pi\hbar^2 a}{m}|\psi|^2\psi$$

$$+\frac{i\hbar}{2}\left(\frac{K_2}{2}|\psi|^2 + \frac{K_3}{6}|\psi|^4\right)\psi$$

K_2, K_3 —— loss-rate coefficients of two- and three-body inelastic collisions

Shell Formation of Collapsing ^{85}Rb BEC

$N_0 = 5 \times 10^4$

$a_{\text{init}} = 20 \text{ nm} \implies a_{\text{collapse}} = -20 \text{ nm}$

10μm

t = 0   t = 5.8   t = 6.6   t = 7.3
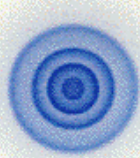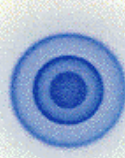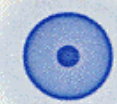
t = 7.9   t = 8.5   t = 8.8   t = 9.1
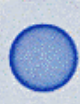
t = 9.3   t = 9.6   t = 9.9   t = 10.2 [ms]
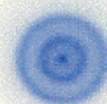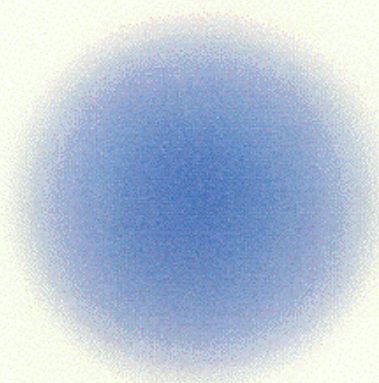
Pattern formation in axisymmetric traps

pancake

$\omega_z/\omega_\perp = \sqrt{8}$

cigar-shape

$\omega_z/\omega_\perp = 0.3$

from z axis

from x axis